# Real-Time Tracking of Curing Process of an Epoxy Adhesive by X-Ray Photon Correlation Spectroscopy

Leonidas Tsapatsaris <sup>1</sup> , Lutz Wiegart <sup>2</sup> , Stanislas Petrash <sup>3</sup> , Tobias Baumeister <sup>5</sup> , Thomas Engels <sup>6</sup> ,
Maya Endoh <sup>1</sup> , Tadanori Koga <sup>1,4,*</sup>
<sup>1</sup> Department of Materials Science and Chemical Engineering, Stony Brook University, New York
11794-2275
<sup>2</sup> National Synchrotron Light Source II, Brookhaven National Laboratory, Upton, New York, 11973
<sup>3</sup> Adhesive Technologies, Henkel Corporation, Bridgewater, New Jersey, 08807
<sup>4</sup> Department of Chemistry, Stony Brook University, Stony Brook, New York, 11794-3400
<sup>5</sup> Henkel AG & Co. KGaA 69123 Heidelberg, Germany
<sup>6</sup> Henkel AG & Co. KGaA 40191 Düsseldorf, Germany

\*Corresponding Author

tadanori.koga@stonybrook.edu (T. K.)

Abstract

In situ X-ray photon correlation spectroscopy (XPCS) was used to investigate the crosslinking

kinetics of a two-component epoxy resin adhesive. The effect of external temperature on the

crosslinking reaction was studied by subjecting the epoxy to different curing temperature profiles.

The temporally resolved dynamics of fillers was tracked, which conveniently served as a probe of

the internal dynamics of the thermoset network and allowed us to study the crosslinking process.

The epoxy resins showed different relaxation processes depending on temperature, indicating a

complex relationship between applied temperature and the development of stress/relaxation

conditions related to the formation of the thermoset network and subsequent vitrification process.

The epoxy was found to be highly temperature sensitive, with heating to elevated temperatures

promoting gelation, but the vitrification process was not completed during the isothermal curing

stage. Instead, cooling the sample to room temperature facilitated the final vitrification process.

Finally, this paper contextualizes the results of this epoxy system within the broader field of XPCS

on complex polymer systems and further advocates for XPCS as a fundamental technique for the

study of complex polymers.

Keywords: X-ray photon correlation spectroscopy, epoxy, curing, network, out-of-equilibrium

2

## Introduction

Cross-linkable polymers are found in nearly every industry, including automotive, aerospace, construction, and microelectronics, and are used in everything from coatings to electronics to adhesives, from consumer applications through the industrial production scale<sup>1-4</sup>. Their widespread use is due to their useful properties, such as thermomechanical toughness, chemical resistance, and adhesive strength<sup>5-8</sup>. As with any useful material, various industries are interested in developing a thorough scientific understanding of why cross-linkable polymers work the way they do, because knowing why they work allows us to make better design and production decisions, tailor the material to specific needs, and develop a more successful product. However, the traditional understanding of cross-linkable polymers — often derived from empirical, time-consuming trial-and-error experiments — is insufficient to capture the complex chemical and physical mechanisms behind these remarkable materials<sup>9, 10</sup>.

Cross-linkable polymers derive their strength from the formation of a three-dimensional crosslinked network that develops as the material undergoes the crosslinking reaction<sup>8</sup>. This reaction is often initiated by an external stimulus, such as heat, UV light, moisture, or another reactant, in a process commonly referred to as "curing"<sup>11-14</sup>. A typical challenge with these materials is the difficulty of performing *in situ/real-time* measurements because the materials often react rapidly and solidify as they cure, making traditional characterization measurements, such as differential scanning calorimetry (DSC) and rheology, difficult. For example, rheology is not useful after the material has finished curing and is macroscopically solid, while DSC is only useful after the material has finished curing<sup>15-18</sup>. Dielectric spectroscopy can measure dynamic processes, such as curing, but it is a bulk measurement like rheology, and lacks the capability to measure at specified length scales. Electron microscopy techniques are useful for characterizing the post-

crosslinked structure, but it is not currently possible to use these techniques to study cross-linkable materials while the crosslinking reaction is occurring<sup>19, 20</sup>. For some polymers, the high energy electron beam used for electron microscopy can actually induce crosslinking – a phenomenon that is much more likely to occur when using an electron beam than, for example, an X-ray beam<sup>21</sup>.

X-ray scattering is uniquely suited to the *in-situ* study of cross-linkable polymers. It's non-destructive, it can elucidate information about the structures and dynamics of a material in real time, and it is equally useful for studying the non-crosslinked precursor materials as it is for the final, fully crosslinked polymer. Small-angle X-ray scattering (SAXS) and wide-angle X-ray scattering (WAXS) are well suited to probe the structure of polymeric materials and have been widely used by the polymer community. However, static scattering signals are only sensitive to changes in the average length scales within the system and can't provide information about the characteristic time scales of the system. For example, the static scattering of a colloid diffusing in a liquid and the same colloid "frozen" in the solid state of the liquid would be fundamentally the same.

Emerging dynamic X-ray scattering techniques such as X-ray photon correlation spectroscopy (XPCS) can provide the spatially and temporally resolved dynamics of materials over relevant time scales (sub-milliseconds to 1000s of seconds) and length scales (nanometers to hundreds of nanometers), making them more useful for complex, out-of-equilibrium systems<sup>22,23</sup>. Furthermore, the recent development of *in-operando* XPCS allows researchers to closely mimic industrial processing conditions, shedding new light on the crosslinking and vitrification process of crosslinkable polymers<sup>3, 4, 12, 24, 25</sup>. Moreover, XPCS is a microbeam scattering technique, with a typical beam diameter of tens of μm, and can probe materials in configurations as close to their real use-

case as possible (e.g., a 100  $\mu$ m thin film sandwiched between two parts), and still provide spatial resolution within that layer<sup>3, 4, 26</sup>.

In this study, XPCS is used for the *in-situ* characterization of the crosslinking kinetics of an industrially relevant two-component epoxy resin adhesive. In addition to providing mechanical and thermal stability to the epoxy resin, nanofillers conveniently act as internal dynamic probes to resolve the evolution of crosslinking by sensing the matrix's mobility<sup>3, 4, 11, 23, 27-30</sup>. We aim to demonstrate diverse and useful information that can be obtained using *in situ* XPCS to study the dynamics of an epoxy resin adhesive as it undergoes a crosslinking reaction.

### **Materials & Methods**

The material of interest in this study was a two-part epoxy structural adhesive supplied by Henkel AG & Co., KGaA. The primary components of the adhesive were epoxy resins and various polyamines, with fumed silica as a thickener, lamellar talc as a viscosity modifier, and carbon black for coloration and viscosity modification. The concentration of silica particles was ~2% (by volume) with a BET surface area of 105-140 m<sup>2</sup>/g, according to ISO 9277. The concentration of CB filler was less than 0.1% by volume. The recommended cure schedule for the adhesive is 8 hours at room temperature, or approximately 15 minutes when heated to 80 °C, for initial strength. According to the manufacturer's specifications, the final strength is achieved after a total cure time of approximately 2 days at room temperature or approximately 30 minutes at 80 °C.

XPCS elucidates the dynamics and changes in dynamics of an out-of-equilibrium system by tracking the changes in the electron density profile through a time series of coherent scattering

patterns. Equilibrium dynamics are quantified by an intensity-intensity autocorrelation function, g<sub>2</sub>, which is derived from the time series of speckle patterns:

$$g_2(q, \Delta t) = \frac{\langle I(q,t)I(q,t+\Delta t)\rangle}{\langle I(q,t)\rangle^2},\tag{1}$$

where q is the scattering vector described by  $q = 4\pi \sin(\theta)/\lambda$  with  $2\theta$  being the scattering angle in the small angle scattering geometry and  $\lambda$  being the wavelength of the incident X-ray beam. I(q) is the scattering intensity recorded on the detector at a given scattering vector, t is the experimental time. The <...> brackets denote an ensemble averaging performed over all detector pixels corresponding to the same scattering vector and over the experimental time<sup>3, 27</sup>. Since Equation (1) is time-averaged, it cannot capture dynamics that are out-of-equilibrium. For example, for a crosslinking epoxy, the dynamics immediately after mixing will not be the same as the dynamics 100 minutes after mixing, so the relevant time scales are not constant and therefore cannot be averaged without losing information. Instead, a two-time correlation function is used, which defines the intensity-intensity autocorrelation function for arbitrary times  $t_1$  and  $t_2$  within a time series, where the ensemble averaging is performed over the pixels belonging to the same scattering vector, but not over time<sup>3, 4, 27</sup>:

$$C(q, t_1, t_2) = \frac{\langle I(q, t_1)I(q, t_2)\rangle}{\langle I(q, t_1)\rangle\langle I(q, t_2)\rangle}$$
(2)

The average elapsed time between two discrete time points in the time series is  $t_{age} = (t_1 + t_2)/2$ , which also represents the elapsed experimental time and is used in this paper to denote the time elapsed after the start of data collection. With  $t_{age}$  and a lag time  $\tau = |t_2 - t_1|$ , one can define an "aged" one-time correlation by averaging the two-time correlation function in Equation (2) around

a given  $t_{age}$ , with the amount of averaging ( $\Delta t_{age}$ ) chosen such that the average is taken over parts of the two-time correlation function that describe "quasi-equilibrium" dynamics:

$$g_{2}(q, t_{age}, \tau) = \frac{\langle I\left(q, t_{age} - \frac{\tau}{2}\right) I\left(q, t_{age} + \frac{\tau}{2}\right) \rangle_{q, t_{age} \pm \Delta t_{age}}}{\langle I\left(q, t_{age} - \frac{\tau}{2}\right) \rangle_{q, t_{age} \pm \Delta t_{age}} * \langle I\left(q, t_{age} + \frac{\tau}{2}\right) \rangle_{q, t_{age} \pm \Delta t_{age}}}$$
(3)

This aged  $g_2$  function (Equation (3)) is fit to a Kohlrausch-Williams-Watts (KWW) form shown in Equation (4) to obtain quantitative information about the dynamics<sup>31-33</sup>:

$$g_2(q, t_{age}, \tau) = A + \beta * e^{-2*(\Gamma * \tau)^{\gamma}} \Big|_{q, t_{age}}$$

$$\tag{4}$$

where  $\beta$  is the optical contrast (also known as the Siegert factor), A is the baseline,  $\Gamma$  is the relaxation rate, and  $\gamma$  is the shape parameter (also known as the stretching exponent)<sup>3, 4, 24, 25, 32</sup>. The setup-dependent optical contrast was determined as  $\beta \approx 0.12$  from measurements of a static reference sample (CoralPor®, Schott) (Figure S1). Full analytical protocols are described in previous reports<sup>3, 4, 34</sup>.

The sample was used as received without further modification. The sample was prepackaged in a two-component cartridge, to which a mixing nozzle could be attached so that the sample could be mixed and extruded simultaneously. As specified by the manufacturer, the cartridge was preheated in an oven at 40 °C for 1 hour prior to use. The sample was extruded *ex situ*, outside of the beamline experimental hutch, through the mixing nozzle into a round sample holder (3 mm diameter and 1.5 mm sample thickness) walled with 25 µm thick polyamide windows (LINQTAPE<sup>TM</sup>, Caplinq). The manual sample handling procedure did not allow us to control the times that elapsed between removal from the oven and extrusion into the sample holder, or between

extrusion into the sample holder and initiation of the measurement. Since the cure kinetics without external heating (i.e., at room temperature) were very slow, and the time periods between when we mixed each epoxy and the start of each sample's respective temperature ramp were comparable, we set the time at which the heating ramp began for each sample as the effective "start time". Therefore,  $t_{age}$  refers to the time elapsed from that point.

Once a sample was mounted in the beamline, its temperature was controlled remotely using a PID-controlled resistive heater. For this adhesive, two specific temperature profiles were of interest: constant temperature at 40 °C, and constant temperature at 80 °C. For the "constant 40 °C" profile, the sample experienced a short heating ramp at the start of the experiment at a rate of 5 °C/min, followed by an extended hold time for about 500 minutes, and finally a short cooling period in which the heater was turned off and the sample was allowed to cool to room temperature (see, Figure S2a for the detailed temperature ramp). For the "constant 80 °C" profile, the sample also experienced a heating ramp at the start of the experiment, but because it had to reach a higher temperature than the 40 °C sample and the ramp rate was set at 5 °C/min, the 80 °C heating ramp took longer. This was followed by a short hold time at 80 °C of about 35 minutes, and finally a cooling period, again induced simply by turning off the heater and allowing the sample to cool to room temperature (see, Figure S2b).

The XPCS experiments were performed at the Coherent Hard X-ray beamline (11-ID) of the National Synchrotron Light Source II at Brookhaven National Laboratory. The partially coherent X-rays had an energy of 9.65 keV ( $\lambda = 0.128$  nanometers), selected by Si (111) double-crystal monochromators. The unattenuated beam flux was  $3x10^{11}$  photons/second, in a 40  $\mu$ m diameter spot at the sample position. Speckle patterns were collected in SAXS transmission geometry using an Eiger X 4M pixelated photon counting detector (Dectris), with a sample-to-detector distance of

16.03 m. The optimal transmission, frame rate, and exposure times were controlled by attenuating the beam using double-sided polished silicon wafers and a millisecond fast shutter. Radiation damage was mitigated by ensuring that no changes in dynamics were induced in the sample from exposure to the X-ray beam over the length of the scan (i.e., the observed dynamics were independent of total X-ray dose and dose rate). In addition, the sample was moved perpendicular to the beam for each XPCS time series so that X-ray dose did not accumulate. A range of frame rates and exposures were used to capture dynamics over a wide range of time scales, from as low as 0.025 seconds by 500 frames for a total 12.5-second time series, to as high as 16.25 seconds by 500 frames for a total 2.25-hour time series. Frame rates, temperature, and motion control were integrated and controlled by the Experimental Physics and Industrial Control System (EPICS) running on a dedicated workstation, which was in communication with the beamline to allow synchronized process control and X-ray scattering data acquisition via the BlueSky data collection framework 35, 36. Calculations of correlation functions were performed using the CHX beamline Python code 34.

Dielectric analysis was performed using a NETZSCH DEA 288 Ionic dielectric analyzer. A typical DEA experiment returns the ion viscosity (IV) of a material as a function of time. For an isothermal DEA experiment, the ion viscosity can be related to the degree of cure ( $\alpha$ ) with the relationship,  $\alpha = k*log(IV) + C^{37}$ , where both k and C are numerical constants. Both components of the epoxy were pre-heated in their unmixed states at 40 °C for 1 hour as specified by the manufacturer. The epoxies were then extruded through a mixing nozzle to begin the curing reaction and placed in the dielectric analyzer. Each DEA experiment was performed isothermally to simplify calculations of the degree of cure. One sample was held at 40 °C, and another was held at 80 °C.

#### **Results & Discussion**

The time-resolved small-angle X-ray scattering (SAXS) curves, I(q), which reflect the structure of the system during the curing reaction, can be obtained by radial averaging of the coherent scattering pattern from the XPCS time series (Figure 1). Figure 1 shows representative SAXS profiles at the early and final stages of curing. The SAXS curve changed subtly, suggesting that the evolution of the filler structure within the experimental time window was minimal. The scattering signal is dominated in the high q regime by a form factor of filler particles, appearing as oscillations at  $q > 0.006 \text{ Å}^{-1}$ . A power-law q dependence (i.e.,  $I(q) \propto q^{-p}$ ) is observed in the low q regime. The particle size of lamellar talc (> 10  $\mu$ m) is larger than the length scales resolved in the q range, so its form factor is not resolved. Silica (SiO<sub>2</sub>) and carbon black (CB) fillers are also mixed in the sample. The SiO<sub>2</sub> particles used here were surface treated to prevent aggregation, which meant they were more uniformly dispersed in the epoxy. Therefore, we attribute the oscillations to a form factor of the relatively monodisperse SiO<sub>2</sub> filler rather than the primary CB filler which are typically fused together<sup>38</sup>. However, the fitting of the I(q) curves was not straightforward; this epoxy was a complicated scattering system due to multiple competing scattering contributions within the observed q range. Hence, we compare the experimental data and a calculated form factor, rather than fitting.

A calculated form factor of spherical SiO<sub>2</sub> particles with a diameter (*D*) of 74 nm and a polydispersity of 15% is shown in Figure 1 (black dashed line). This calculated form factor reasonably expresses the shapes and peak positions of the three peaks located at approximately  $q = 0.009 \text{ Å}^{-1}$ ,  $0.016 \text{ Å}^{-1}$ , and  $0.023 \text{ Å}^{-1}$  in the experimental data. An "apparent" power law with an exponent p = -3.2 is observed in the low q regime. The exponent is "apparent" because the contributions from the form factor at  $q = 0.009 \text{ Å}^{-1}$  influence the scattering curve at low q, so it is

not solely a pure power-law fit in the low q regime. We expect this power-law contribution to come from a surface fractal structure of the talc. Since a detailed discussion of the nanoparticle structure is beyond our current interest, these questions deserve future work. In any case, we chose to limit the evaluation of the XPCS data to  $q > 0.006 \text{ Å}^{-1}$ , which is above the q-region that is affected by scattering from the talc and/or aggregates of SiO<sub>2</sub> and CB, to minimize any possible influence from these structures on the dynamics. Therefore, we ensured that the dynamics discussed herein are mainly from the primary SiO<sub>2</sub> fillers.

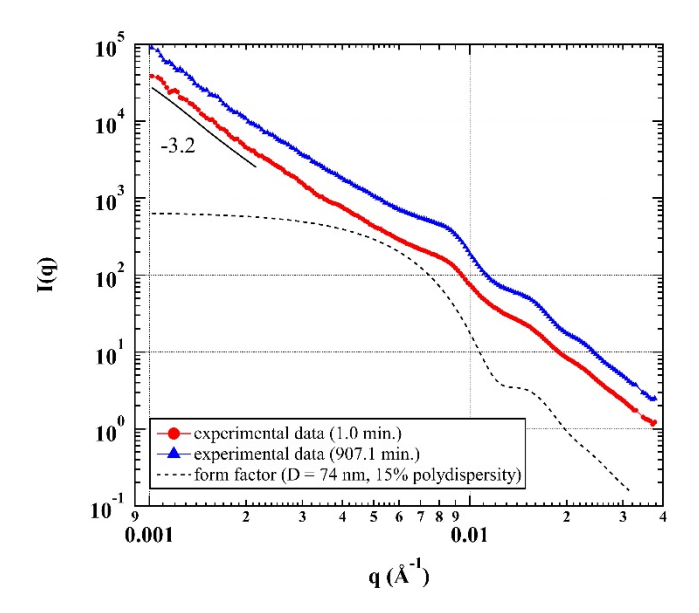


Figure 1. SAXS curves of the epoxy cured at 40 °C, shown at  $t_{age}$  = 1.0 min. and  $t_{age}$  = 907.1 min. The black dashed line is the form factor of the SiO<sub>2</sub> filler. Curves are arbitrarily shifted for readability. The gap in each curve at  $q \approx 0.033$  Å<sup>-1</sup> is due to removing a diffraction peak resulting from the beam stop that was not relevant to the material studied here.

We studied the out-of-equilibrium dynamics of the epoxy during the curing process. Figure 2 shows two XPCS two-time correlation functions that are representative of the curing process. Each two-time correlation function in Figure 2 reflects dynamics in the curing material over a particular

range of times. It is essential to note that the two-time correlation functions represent dynamics of the primary scatterers, i.e., the SiO<sub>2</sub> filler particles (see Figure 1), which in turn are affected by the evolving dynamics of the curing epoxy. The right panel of Figure 2 depicts a later stage in the curing process, where the combination of X-ray exposure time and number of frames allowed us to capture the crosslinking dynamics in such a way that they appeared to be in "quasi-equilibrium", represented as a straight, diagonal shape of the two-time correlation function. Therefore, for the duration of the scan, the filler particle dynamics slowed only slightly, implying that the rate of the epoxy's crosslinking dynamics also slowed only slightly, and analysis of the two-time correlation function with Eq. (3) and (4) was relatively straightforward. In contrast, and much less frequently, the dynamics of the epoxy appeared to be "out-of-equilibrium". The left panel of Figure 2 depicts these "out-of-equilibrium" dynamics at an earlier stage in the curing process. In this time series, the range of lag times over which there is strong correlation (yellow color in Figure 2) was rapidly decreasing with increasing experimental time; the rapid loss of correlation with experimental time indicates that the epoxy's crosslinking dynamics were speeding up. During this time series, the sample temperature was increasing due to the initial ramp up in the temperature profile, which explains the dynamics speeding up. To analyze time series like this one, a small  $\Delta t_{age}$  is chosen over which to calculate the one-time correlation function. This  $\Delta t_{age}$  should ideally cover a range in the time series that is approximately quasi-equilibrium (e.g., 40-60 seconds in the left panel of Figure 2).

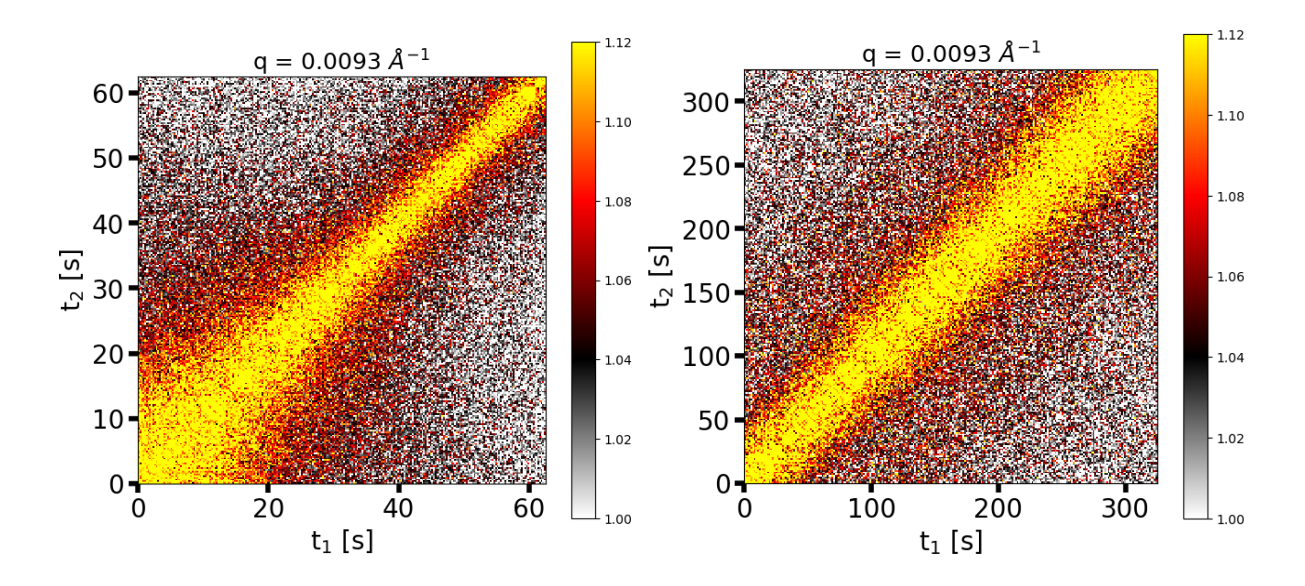


Figure 2. Two-time correlation functions of the adhesive cured at 40 °C; (left) "out-of-equilibrium" dynamics; (right) "quasi-equilibrium" dynamics.

In Figure 3, we plot a series of evolving one-time correlation functions selected at various times, with a representative q value of q = 0.0093 Å<sup>-1</sup>. Here,  $g_2$  is normalized as  $(g_2 - A)/\beta$  so that the decay progresses from an initial value of 1 to a final baseline value of 0. For both temperature runs, we captured the dynamics with lag times  $(\tau)$  extending up to 5000 seconds, at aging times well after the epoxy had fully solidified macroscopically. Interestingly, for both temperature conditions, decorrelation in  $g_2$  was still observed at very long aging times  $(t_{age}=767.1 \text{ min. for } 40 \,^{\circ}\text{C}, t_{age}=772.8 \,^{\circ}\text{min. for } 80\,^{\circ}\text{C})$ . Previous work<sup>39-41</sup> proposed that a q-independent value of the stretching exponent  $(\gamma)$  greater than 1 is indicative of deformation due to the relaxation of internal stresses built up during the curing reaction (see Figure 4 and Figure S3). This relaxation can cause a complete decay of  $g_2$ , even for fully developed solids. It is this relaxation process that is responsible for the decay of the one-time correlation function over the lag time  $\tau > 10^3$  seconds seen in Figure 3. We did not observe complete decorrelation at these late times because a scan to resolve the decorrelation

would itself take longer than  $10^3$  seconds. It is not justified to quantitatively discuss incomplete  $g_2$  decay using a fit of the KWW equation, so these late aging times are not included in further discussions pertaining to the KWW fitting parameters. These results are consistent with the manufacturer's claim that the epoxy takes up to 48 hours to fully cure. Hence, XPCS is a powerful technique that can reliably track these slow dynamics in macroscopically solidified materials such as this epoxy resin.

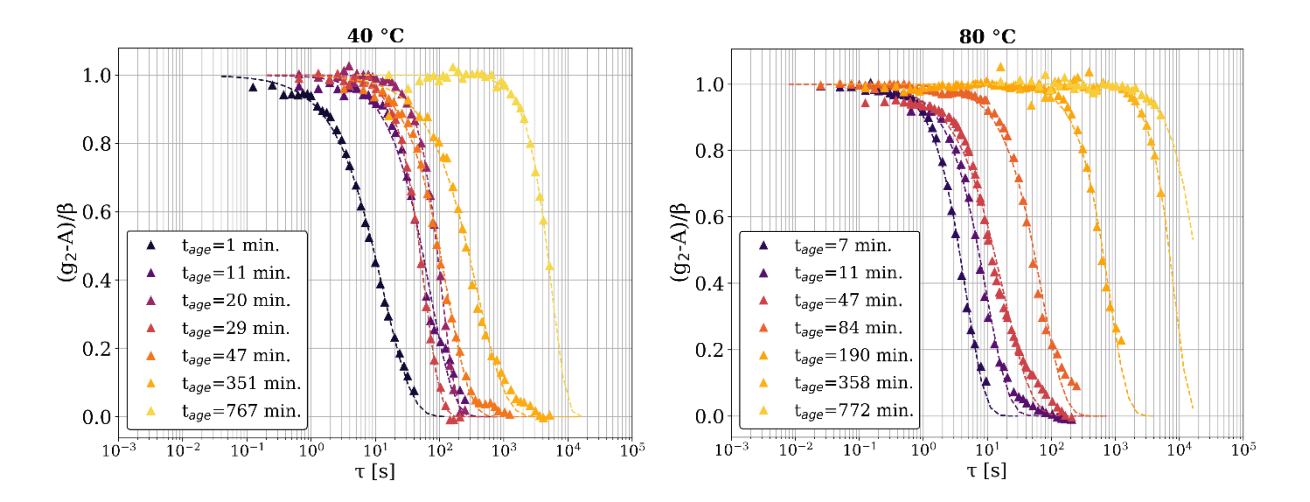


Figure 3. Fits of the KWW equation to the normalized one-time correlation functions ( $g_2$ ) at q = 0.0093  $Å^{-1}$ ; (left) 40 °C sample, (right) 80 °C sample. The triangular points are the correlation function data, and the dashed lines are the fits of the KWW equation. The legend shows the time at which each correlation function was calculated.

We studied the curing process of the epoxy through changes in the physical properties of the epoxy by fitting the KWW equation (Eq. (4)) to the one-time correlation function  $(g_2)$ . The stretch/compression exponent  $(\gamma)$  determines the shape of the  $g_2$  curve and provides insight into the type of dynamics exhibited by the SiO<sub>2</sub> filler particles as the epoxy cures. Through the interactions

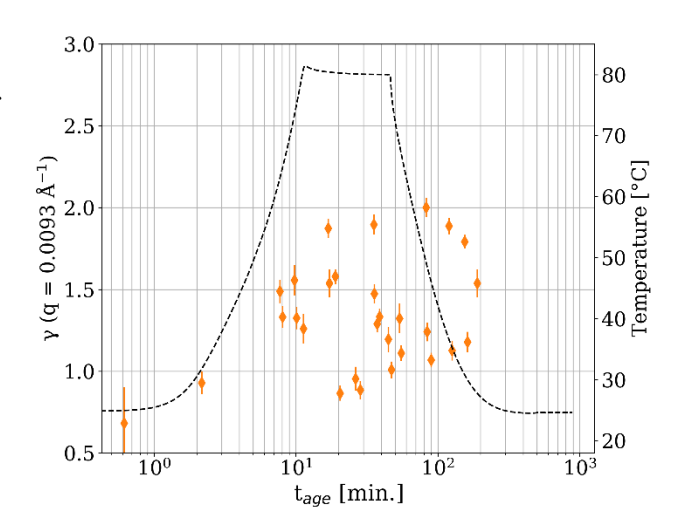


Figure 4. Stretching exponent ( $\gamma$ ) versus time after mixing for the 80 °C sample. The dashed line shows the temperature metadata.

between the filler particles and the thermoset network, the  $\gamma$  exponent characterizes the overall dynamics of the epoxy, with  $\gamma < 1$  indicating sub-diffusive dynamics and  $\gamma > 1$  indicating hyper-diffusive dynamics<sup>29, 42</sup>.

Figure 4 shows the time dependence of  $\gamma$  for the 80 °C sample. At  $t_{age}$  < 10 minutes,  $\gamma$  was less than 1, which represents sub-diffusive dynamics and is attributed to the emergence of multiple relaxation processes in the disordered system<sup>43</sup>. However, after  $t_{age}$  = 10 minutes, the value of  $\gamma$  quickly became difficult to describe with a conclusive pattern due to high variability with  $t_{age}$ . At the beginning of the temperature ramp,  $\gamma$  became greater than 1 and began to approach  $\gamma$  = 1.5 or higher, representing hyper-diffusive dynamics and indicating that the relaxation becomes compressed (i.e., faster than an exponential decay). We previously reported that a change of  $\gamma$  from 1 (the least stressed state, i.e., no epoxy network formation) to 1.5 <  $\gamma$  < 2.0 is associated with the onset of epoxy network formation (i.e., gelation)<sup>3, 4, 26</sup>. Therefore, it appears that the formation of the thermoset network started around  $t_{age}$  = 10 min. for the 80 °C sample. After this point,  $\gamma$  fluctuated significantly until  $t_{age} \approx 200$  min., suggesting some stress relief in the network associated

with thermally induced curing<sup>3, 4, 26</sup>. Cipelletti et al.<sup>40</sup> proposed that a compression exponent less than 2 is indicative of a wide distribution of ballistic relaxation times. In this epoxy the value of  $\gamma$  fluctuates considerably, but remains less than 2, which, in combination with the curing dynamics described below (Figure 6), may represent stress relief seen as a range of relaxation times. The observed value of  $\gamma$  was found to be almost independent of q for multiple values of  $t_{age}$  (Figure S3). For the 40 °C sample,  $\gamma$  was also less than one before the onset of heating (Figure S4), but the transition from  $\gamma = 1$  to  $1.5 < \gamma < 2.0$  was not so clear. Like the 80 °C sample, there was a lot of variability in  $\gamma$  over  $t_{age}$ , making it difficult to discern a pattern. However,  $\gamma$  generally remained below 2, also pointing towards the same stress relief associated with curing that was seen for the 80 °C sample. Though there were notable exceptions around  $t_{age} = 20$  minutes, which makes drawing a conclusion difficult. Generally, such hyper-diffusive dynamics, characterized by  $\gamma > 1$ , are a common feature in the aging regime of soft condensed matter systems<sup>39, 40, 44-46</sup>. Further XPCS experiments on this material at different temperatures would help elucidate this difference and deserve future work.

For soft matter systems, the relationship between the relaxation rate ( $\Gamma$ ) and q is of interest because it indicates whether the observed dynamics are diffusive or ballistic<sup>27</sup>. As shown in Figure 5, the epoxy shows linear scaling between  $\Gamma$  and q for both the 40 °C and the 80 °C samples throughout the experiment. Linear scaling between  $\Gamma$  and q has been observed for colloidal gels, concentrated emulsions, and nanoparticles suspended in polymer matrices<sup>27, 39, 40, 47</sup>. The linear scaling coupled with a compressed exponential of  $\gamma = 1.5$  represents collective, ballistic dynamics resulting from the release of micro-stresses generated in the internal structure of the sample<sup>40</sup>. The lines in Figure 5 show the best fits to the experimental data where  $\Gamma = v_d q$ . In this equation,  $v_d$  is a proportionality constant representing the linear, ballistic motion of scatterers as a local

displacement velocity with units of  $Å/s^3$ , 4, 26. The samples at both curing temperatures show progressively slower dynamics as the time increases (i.e., as the crosslinking reaction takes place).

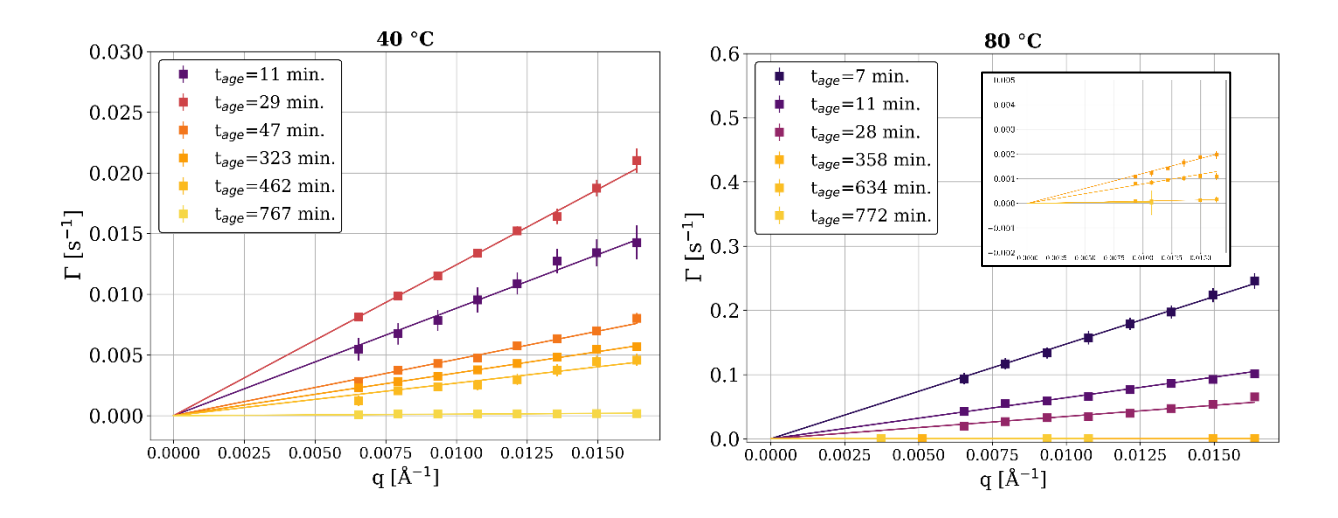


Figure 5. Relaxation rate ( $\Gamma$ ) as a function of the scattering vector (q) for a range of times, at 40 °C and 80 °C. The inset in the right image is a "zoomed in" view of the later  $t_{age}$  relaxation rates.

The displacement velocity ( $v_d$ ) is a key quantity in the study of epoxy's curing kinetics. It describes the linear displacement dynamics resulting from the interaction between the filler and the polymer matrix and is independent of length scale (as seen in Figure 5)<sup>4</sup>. The displacement velocity is plotted as a function of time in **Error! Reference source not found.**. The formation of the crosslink network (i.e., gelation) can be observed for both samples starting before  $t_{age}=10 \text{ min.}$ , as the  $v_d$  of both samples started to decay with a power-law exponent (m) of around -1 (i.e.,  $v_d \propto$ 

 $t_{age}^{m}$ ). We previously reported an m = -2 power-law decay in similar industrial epoxy samples<sup>3, 4, 26</sup>, implying this epoxy cures relatively slowly at the isothermal condition. This power-law decay is marked with the m = -1 black dashed lines in Figure 6. The displacement velocity of the 40 °C sample was lower than the v<sub>d</sub> of the 80 °C sample from  $t_{age} \approx 10$  min. up to  $t_{age} \approx 50$  min. This is attributed to the fact that the 80 °C sample was heated to a higher temperature and

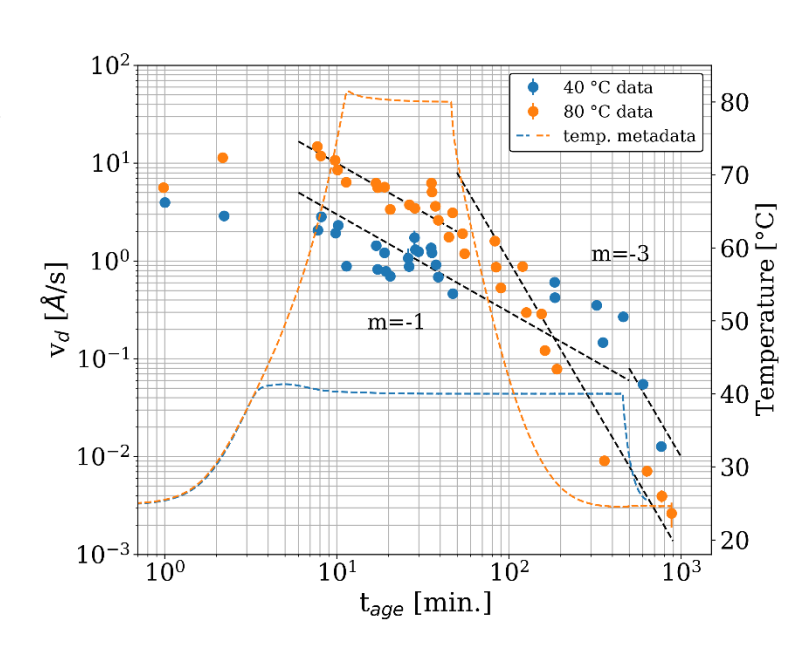


Figure 6. Displacement velocity as a function of time (colored points), with temperature metadata included for reference (dashed lines). The data are the same color as the corresponding temperature profile. Dashed black lines show the power-law trend with the corresponding power law exponent (m).

was subject to a temperature ramp for longer; the 40 °C sample reached its isothermal condition at  $t_{age} = 5$  min., whereas the 80 °C sample reached its isothermal condition at  $t_{age} \approx 13$  min. The higher temperature and prolonged temperature ramp of the 80 °C sample induced more molecular motion

in the network structure of the epoxy, which is reflected in a larger displacement velocity from faster dynamics of the 80 °C sample's filler particles. Then, during the isothermal phase of each temperature profile, the displacement velocity of the filler particles in both samples gradually decreased at a roughly similar rate of decay. According to the manufacturer's specifications, the final strength is achieved after a total cure time of approximately 30 min during the isothermal reaction at 80 °C, which corresponds to the reaction conversion of approximately 90% ( $\alpha = 0.9$ ) based on conventional dielectric analysis (DEA) results (Figure S5). However, as shown in Figure 6, the displacement velocity after curing at 80 °C for 30 minutes was as fast as the initial state ( $t_{age} = 1 \text{ min.}$ , before the start of gelation). As the temperature was lowered from 80 °C to room temperature,  $v_d$  decreased by nearly three orders of magnitude, showing a power-law decay of  $m \approx -3$ . This is marked by the m = -3 black dashed lines in Figure 6. Similar rapid decay of  $v_d$  was observed when industrial dual-cure acrylate/epoxy thermosets were cured with ultraviolet light<sup>3, 4, 4, 4</sup>. Therefore, this cooling process is expected to accelerate the vitrification process of the epoxy resin used in this study.

A similar trend was observed with the isothermal curing at 40 °C. According to the manufacturer's specifications, at 40 °C (ambient temperature in tropical climates) the epoxy should be cured for approximately 9 hours prior to practical use. Figure S5 shows the DEA results for the epoxy resins cured at 40 °C and 80°C. From the figure, we can see that curing for 450 min at 40 °C allowed us to achieve a reaction conversion of about 85% ( $\alpha = 0.85$ ). However, as shown in Figure 6, the  $v_d$  of the epoxy at 450 min. was 0.5 Å/s. This was still at least two orders-of-magnitude greater than that of the 80 °C sample at  $t_{age} = 900$  min., suggesting that the vitrification process of the 40 °C sample was not complete during this 450-minute isothermal curing process. Again, and as we saw for the isothermal curing at 80°C, the vitrification occurred only after cooling

to room temperature. This cooling-induced vitrification process of the epoxy resin, which cannot be identified by DEA alone, clearly demonstrates the additional data that can be obtained with XPCS alongside conventional technique for studying the complicated gelation/vitrification process of epoxy resins.

Enns and Gillham proposed a time-temperature-transformation (TTT) diagram that predicts gelation and vitrification as a function of cure time and temperature<sup>48</sup>. According to their TTT diagram, epoxy resins are expected to undergo gelation and then vitrification as the cure time increases at a given cure temperature. It should be noted that if the cure temperature is too high, the epoxy resin will degrade without vitrification, and if the cure temperature is too low, the epoxy resin will vitrify without gelation. Therefore, it is extremely important to optimize a cure temperature to achieve the desired final strength of an epoxy, keeping in mind that curing at "room temperature" (roughly in the 20°C to 40°C range, depending on the local ambient climate conditions) is desirable for the customer. The TTT phase diagram for this epoxy is not available, but the XPCS results show that the v<sub>d</sub> gradually decreased over time during the two isothermal curing conditions, indicating a prolonged vitrification process at the microscopic scale. For both epoxy samples, cooling from the isothermal set point drastically decreased the v<sub>d</sub>, reducing the overall curing time at each temperature. Similar industrial epoxies reported previously<sup>3, 4, 26</sup> did not show such rapid decreases in displacement velocity when the temperature was reduced, suggesting that they were relatively temperature insensitive. This commercial epoxy's temperature sensitivity is what ultimately allowed it to meet the curing time and "room temperature" design criteria specified by the manufacturer: ~9 hours at 40 °C, or 30 minutes at 80 °C. If the epoxy were cured isothermally, e.g., at 40 °C, with no cooling, the time required to reach a sufficiently cured state would likely be much larger than what was observed with XPCS, as seen in the DEA

experiments (Figure S5). The mechanism behind the temperature sensitivity of this epoxy is beyond the scope of this paper, but it would be a promising direction for future work.

### **Conclusion**

XPCS allows for experiments on time and length scales that are inaccessible with conventional techniques. For example, rheology can be used to obtain experimental results with comparable time resolution, but in the case of curable adhesives, the rheometer would seize up and stop working, while XPCS could continue to extract meaningful data long beyond this point. This experiment was an example of such, where the cure kinetics were analyzed up to 12 hours after the epoxy resin components were mixed; a point when the epoxy is macroscopically fully solid. Another challenge in studying cross-linkable polymers under industrial application conditions is the need for spatial resolution, as crosslinking reactions often proceed in a spatially heterogeneous manner due to boundary conditions (e.g., proximity to interfaces) – another benefit granted by XPCS. XPCS experiments can also be configured to mimic a variety of industrial conditions, including *ex-situ*, *in-situ*, or *in-operando* mixing.

We leveraged these benefits of XPCS to study a range of useful and physically relevant metrics of our commercial epoxy resin, such as the time it took for the epoxy to cure and how this was affected by the applied temperature, the type of dynamics exhibited by the nanoparticle filler markers, and the relaxation modes present in the epoxy as it cured. The crosslinking kinetics of the epoxy were resolved for more than 12 hours after mixing, using the scattering of the SiO<sub>2</sub> filler and the interactions between the thermoset network and the filler to track the crosslinking kinetics of the epoxy. The type of the filler dynamics was confirmed to be ballistic, as expected based on previous literature results for crosslinking polymers<sup>3, 4, 11, 26</sup>. Our data indicate that the filler

dynamics are comparable within one order-of-magnitude before and after the isothermal temperature condition was reached, indicating a similarity in dynamics between the pre-gelation and post-gelation epoxy resins. The displacement velocity during the isothermal curing portion of both temperature profiles did not decrease as much as was expected. The subsequent cooling to room temperature induced a secondary rapid decay process, and the filler dynamics were found to undergo a transition from a power-law exponent (m) of -1 to m = -3 with aging time. A dynamics-property correlation is a promising avenue for future work. This sample fits well into the broader context of cross-linkable polymers. Its trends in displacement velocity, its relaxation modes ( $\gamma$ ), and its ballistic dynamics show a high degree of similarity to previous work on similar crosslinking polymers<sup>3, 4, 11, 24-26</sup>. For these reasons, XPCS should be considered a "go-to" technique for the study of industrially relevant and complex polymer systems under out-of-equilibrium conditions.

# Acknowledgements

T.K. acknowledges partial financial support from the National Science Foundation (DMR 2210207 and DGE 1922639). This work used resources of the National Synchrotron Light Source-II (Beamline 11-ID), which is a U.S. DOE Office of Science Facility at Brookhaven National Laboratory under Contract No. DE-SC0012704.

#### **Conflicts of Interest**

Author Stanislas Petrash is employed by Henkel Corporation, United States. Authors Tobias Baumeister and Thomas Engels are employed by Henkel AG & Co., Germany. The remaining authors declare that the research was conducted in the absence of any commercial or financial relationships that could be construed as a potential conflict of interest.

### References

- (1) Sahagun, C. M.; Morgan, S. E. Thermal Control of Nanostructure and Molecular Network Development in Epoxy-Amine Thermosets. *ACS Appl. Mater. Interfaces* **2012**, *4* (2), 564-572. DOI: 10.1021/am201515y.
- (2) Jin, F.-L.; Li, X.; Park, S.-J. Synthesis and application of epoxy resins: A review. *Journal of Industrial and Engineering Chemistry* **2015**, *29*, 1-11. DOI: 10.1016/j.jiec.2015.03.026.
- (3) Yavitt, B. M.; Salatto, D.; Huang, Z.; Koga, Y. T.; Endoh, M. K.; Wiegart, L.; Poeller, S.; Petrash, S.; Koga, T. Revealing nanoscale dynamics during an epoxy curing reaction with x-ray photon correlation spectroscopy. *Journal of Applied Physics* **2020**, *127* (11), 114701. DOI: 10.1063/1.5141488.
- (4) Yavitt, B. M.; Wiegart, L.; Salatto, D.; Huang, Z.; Tsapatsaris, L.; Endoh, M. K.; Poeller, S.; Schiel, M.; Petrash, S.; Koga, T. Spatial-Temporal Dynamics at the Interface of 3D-Printed Photocurable Thermoset Resin Layers. *ACS Appl. Eng. Mater.* **2023**, *1* (2), 868-876. DOI: 10.1021/acsaenm.2c00248.
- (5) Sprenger, S. Epoxy resin composites with surface-modified silicon dioxide nanoparticles: A review. *Journal of Applied Polymer Science* 2013, 130 (3), 1421-1428. DOI: 10.1002/app.39208.
- (6) Morsch, S.; Liu, Y.; Greensmith, P.; Lyon, S. B.; Gibbon, S. R. Molecularly controlled epoxy network nanostructures. *Polymer* **2017**, *108*, 146-153. DOI: 10.1016/j.polymer.2016.11.050.
- (7) Morsch, S.; Liu, Y.; Lyon, S. B.; Gibbon, S. R. Insights into Epoxy Network Nanostructural Heterogeneity Using AFM-IR. *ACS Appl. Mater. Interfaces* **2016**, *8* (1), 959-966. DOI: 10.1021/acsami.5b10767.

- (8) Nair, C. P. R. Advances in addition-cure phenolic resins. *Progress in Polymer Science* **2004**, *29* (5), 401-498. DOI: 10.1016/j.progpolymsci.2004.01.004.
- (9) Sharifi, M.; Jang, C. W.; Abrams, C. F.; Palmese, G. R. Toughened epoxy polymers via rearrangement of network topology. *J. Mater. Chem. A* **2014**, *2* (38), 16071-16082. DOI: 10.1039/C4TA03051F.
- (10) Min, B. G.; Hodgkin, J. H.; Stachurski, Z. H. The dependence of fracture properties on cure temperature in a DGEBA/DDS epoxy system. *Journal of Applied Polymer Science* **1993**, 48 (7), 1303-1312. DOI: 10.1002/app.1993.070480719.
- (11) Trigg, E. B.; Wiegart, L.; Fluerasu, A.; Koerner, H. Dynamics of Polymerization and Gelation in Epoxy Nanocomposites via X-ray Photon Correlation Spectroscopy.

  \*Macromolecules 2021, 54 (13), 6575-6584. DOI: 10.1021/acs.macromol.1c00727.
- (12) Ehrburger-Dolle, F.; Morfin, I.; Bley, F.; Livet, F.; Heinrich, G.; Chushkin, Y.; Sutton, M. Anisotropic and heterogeneous dynamics in stretched elastomer nanocomposites. *Soft Matter* **2019**, *15* (18), 3796-3806. DOI: 10.1039/C8SM02289E.
- (13) Araki, W.; Adachi, T.; Gamou, M.; Yamaji, A. Time–Temperature Dependence of Fracture

  Toughness for Bisphenol A Epoxy Resin. *Proceedings of The Institution of Mechanical*Engineers Part L-journal of Materials-design and Applications PROC I 2002, 216, 79
  84. DOI: 10.1243/146442002320139289.
- (14) Araki, W.; Adachi, T.; Yamaji, A.; Gamou, M. Fracture toughness of bisphenol A-type epoxy resin. *Journal of Applied Polymer Science* **2002**, *86* (9), 2266-2271. DOI: 10.1002/app.11208.
- (15) Schlosser, E.; Schönhals, A. Recent development in dielectric relaxation spectroscopy of polymers. *Colloid & Polymer Sci* **1989**, *267* (11), 963-969. DOI: 10.1007/BF01410156.

- (16) Ellis, B. The kinetics of cure and network formation. In *Chemistry and Technology of Epoxy Resins*, Ellis, B. Ed.; Springer Netherlands, 1993; pp 72-116.
- (17) Estridge, C. E. The effects of competitive primary and secondary amine reactivity on the structural evolution and properties of an epoxy thermoset resin during cure: A molecular dynamics study. *Polymer* **2018**, *141*, 12-20. DOI: 10.1016/j.polymer.2018.02.062.
- (18) Bahrami, A.; Morelle, X.; Hông Minh, L. D.; Pardoen, T.; Bailly, C.; Nysten, B. Curing dependent spatial heterogeneity of mechanical response in epoxy resins revealed by atomic force microscopy. *Polymer* **2015**, *68*, 1-10. DOI: 10.1016/j.polymer.2015.04.084.
- (19) Kishi, H.; Naitou, T.; Matsuda, S.; Murakami, A.; Muraji, Y.; Nakagawa, Y. Mechanical properties and inhomogeneous nanostructures of dicyandiamide-cured epoxy resins.

  \*\*Journal of Polymer Science Part B: Polymer Physics 2007, 45 (12), 1425-1434. DOI: 10.1002/polb.21170.
- (20) Gu, X.; Raghavan, D.; Ho, D. L.; Sung, L.; VanLandingham, M. R.; Nguyen, T.
  Nanocharacterization of Surface and Interface of Different Epoxy Networks. MRS Online
  Proceedings Library 2011, 710 (1), 1091. DOI: 10.1557/PROC-710-DD10.9.1.
- (21) Gupta, T.; Strelcov, E.; Holland, G.; Schumacher, J.; Yang, Y.; Esch, M. B.; Aksyuk, V.; Zeller, P.; Amati, M.; Gregoratti, L.; et al. Electron and X-ray Focused Beam-Induced Cross-Linking in Liquids: Toward Rapid Continuous 3D Nanoprinting and Interfacing using Soft Materials. ACS Nano 2020, 14 (10), 12982-12992. DOI: 10.1021/acsnano.0c04266.
- (22) Johnson, K. J.; Wiegart, L.; Abbott, A. C.; Johnson, E. B.; Baur, J. W.; Koerner, H. In Operando Monitoring of Dynamic Recovery in 3D-Printed Thermoset Nanocomposites by XPCS. *Langmuir* **2019**, *35* (26), 8758-8768. DOI: 10.1021/acs.langmuir.9b00766.

- (23) Lehmkühler, F.; Roseker, W.; Grübel, G. From Femtoseconds to Hours—Measuring
   Dynamics over 18 Orders of Magnitude with Coherent X-rays. *Applied Sciences* 2021, *11* (13), 6179. DOI: 10.3390/app11136179.
- (24) Andrews, R. N.; Narayanan, S.; Zhang, F.; Kuzmenko, I.; Ilavsky, J. Inverse transformation: unleashing spatially heterogeneous dynamics with an alternative approach to XPCS data analysis. *J Appl Cryst* **2018**, *51* (1), 35-46. DOI: 10.1107/S1600576717015795.
- (25) Hoshino, T.; Okamoto, Y.; Yamamoto, A.; Masunaga, H. Heterogeneous dynamics in the curing process of epoxy resins. *Sci Rep* **2021**, *11* (1), 9767. DOI: 10.1038/s41598-021-89155-x.
- (26) Yavitt, B. M.; Wiegart, L.; Salatto, D.; Huang, Z.; Endoh, M. K.; Poeller, S.; Petrash, S.; Koga, T. Structural Dynamics in UV Curable Resins Resolved by In Situ 3D Printing X-ray Photon Correlation Spectroscopy. ACS Appl. Polym. Mater. 2020, 2 (9), 4096-4108.
  DOI: 10.1021/acsapm.0c00716.
- (27) Fluerasu, A.; Moussaïd, A.; Madsen, A.; Schofield, A. Slow dynamics and aging in colloidal gels studied by x-ray photon correlation spectroscopy. *Phys. Rev. E* 2007, 76
  (1), 010401. DOI: 10.1103/PhysRevE.76.010401.
- (28) Koga, T.; Li, C.; Endoh, M. K.; Koo, J.; Rafailovich, M.; Narayanan, S.; Lee, D. R.; Lurio, L. B.; Sinha, S. K. Reduced Viscosity of the Free Surface in Entangled Polymer Melt Films. *Phys. Rev. Lett.* **2010**, *104* (6), 066101. DOI: 10.1103/PhysRevLett.104.066101.
- (29) Guo, H.; Bourret, G.; Corbierre, M. K.; Rucareanu, S.; Lennox, R. B.; Laaziri, K.; Piche, L.; Sutton, M.; Harden, J. L.; Leheny, R. L. Nanoparticle Motion within Glassy Polymer Melts. *Phys. Rev. Lett.* **2009**, *102* (7), 075702. DOI: 10.1103/PhysRevLett.102.075702.

- (30) Mangal, R.; Srivastava, S.; Narayanan, S.; Archer, L. A. Size-Dependent Particle Dynamics in Entangled Polymer Nanocomposites. *Langmuir* 2016, 32 (2), 596-603. DOI: 10.1021/acs.langmuir.5b03311.
- (31) Williams, G.; Watts, D. C. Non-symmetrical dielectric relaxation behaviour arising from a simple empirical decay function. *Trans. Faraday Soc.* **1970**, *66* (0), 80-85. DOI: 10.1039/TF9706600080.
- (32) Siegert, A. J. F. *On the fluctuations in signals returned by many independently moving scatterers*; Radiation Laboratory, Massachusetts Institute of Technology, 1943.
- (33) Kohlrausch, R. Theorie des elektrischen Rückstandes in der Leidener Flasche. *Annalen der Physik* **1854**, *167* (1), 56-82. DOI: 10.1002/andp.18541670103.
- (34) Abeykoon, S. K.; Zhang, Y.; Dill, E. D.; Caswell, T. A.; Allan, D. B.; Akilic, A.; Wiegart, L.; Wilkins, S.; Heroux, A.; van Dam, K. K.; et al. Software tools for X-ray photon correlation and X-ray speckle visibility spectroscopy. In 2016 New York Scientific Data Summit (NYSDS), 2016/08//, 2016; pp 1-10. DOI: 10.1109/NYSDS.2016.7747815.
- (35) EPICS Experimental Physics and Industrial Control System.
- (36) Bluesky Data Collection Framework bluesky 1.6.7.post2+g888716e documentation.
- (37) Pascault, J. P.; Williams, R. J. J. Glass transition temperature versus conversion relationships for thermosetting polymers. *Journal of Polymer Science Part B: Polymer Physics* **1990**, *28* (1), 85-95. DOI: 10.1002/polb.1990.090280107.
- (38) Koga, T.; Hashimoto, T.; Takenaka, M.; Aizawa, K.; Amino, N.; Nakamura, M.; Yamaguchi, D.; Koizumi, S. New Insight into Hierarchical Structures of Carbon Black Dispersed in Polymer Matrices: A Combined Small-Angle Scattering Study.
  Macromolecules 2008, 41 (2), 453-464. DOI: 10.1021/ma0718671.

- (39) Cipelletti, L.; Manley, S.; Ball, R. C.; Weitz, D. A. Universal Aging Features in the Restructuring of Fractal Colloidal Gels. *Phys. Rev. Lett.* **2000**, *84* (10), 2275-2278. DOI: 10.1103/PhysRevLett.84.2275.
- (40) Cipelletti, L.; Ramos, L.; Manley, S.; Pitard, E.; Weitz, D. A.; Pashkovski, E. E.; Johansson,
  M. Universal non-diffusive slow dynamics in aging soft matter. *Faraday Discuss.* 2003,
  123 (0), 237-251. DOI: 10.1039/B204495A.
- (41) Kwaśniewski, P.; Fluerasu, A.; Madsen, A. Anomalous dynamics at the hard-sphere glass transition. *Soft Matter* **2014**, *10* (43), 8698-8704. DOI: 10.1039/C4SM01671H.
- (42) Jang, W.-S.; Koo, P.; Bryson, K.; Narayanan, S.; Sandy, A.; Russell, T. P.; Mochrie, S. G. Dynamics of Cadmium Sulfide Nanoparticles within Polystyrene Melts. *Macromolecules* **2014**, *47* (18), 6483-6490. DOI: 10.1021/ma500956b.
- (43) Johnston, D. C. Stretched exponential relaxation arising from a continuous sum of exponential decays. *Phys. Rev. B* **2006**, *74* (18), 184430. DOI: 10.1103/PhysRevB.74.184430.
- (44) Bellour, M.; Knaebel, A.; Harden, J. L.; Lequeux, F.; Munch, J. P. Aging processes and scale dependence in soft glassy colloidal suspensions. *Phys. Rev. E* **2003**, *67* (3), 031405. DOI: 10.1103/PhysRevE.67.031405.
- (45) Kaloun, S.; Skouri, R.; Skouri, M.; Munch, J. P.; Schosseler, F. Successive exponential and full aging regimes evidenced by tracer diffusion in a colloidal glass. *Phys. Rev. E* **2005**, 72 (1), 011403. DOI: 10.1103/PhysRevE.72.011403.
- (46) Robert, A.; Wandersman, E.; Dubois, E.; Dupuis, V.; Perzynski, R. Glassy dynamics and aging in a dense ferrofluid. *EPL* **2006**, *75* (5), 764. DOI: 10.1209/epl/i2006-10179-4.

- (47) Bandyopadhyay, R.; Liang, D.; Yardimci, H.; Sessoms, D. A.; Borthwick, M. A.; Mochrie,
  S. G. J.; Harden, J. L.; Leheny, R. L. Evolution of Particle-Scale Dynamics in an Aging
  Clay Suspension. *Phys. Rev. Lett.* 2004, 93 (22), 228302. DOI:
  10.1103/PhysRevLett.93.228302.
- (48) Enns, J. B.; Gillham, J. K. Time–temperature–transformation (TTT) cure diagram:
  Modeling the cure behavior of thermosets. *Journal of Applied Polymer Science* 1983, 28
  (8), 2567-2591. DOI: 10.1002/app.1983.070280810.